Trajectory measurements and correlations in the final focus beam line at the KEK Accelerator Test Facility

Y. Renier and P. Bambade
LAL, Université Paris-Sud, CNRS/IN2P3, Orsay, France

T. Tauchi
High Energy Accelerator Research Organization, Tsukuba, Japan

G. R. White
SLAC National Accelerator Laboratory, Menlo Park, California 94025, USA

S. Boogert
John Adams Institute at RHUL, London, United Kingdom

(Received 2 May 2011; revised manuscript received 12 April 2013; published 28 June 2013)

The Accelerator Test Facility 2 (ATF2) commissioning group aims to demonstrate the feasibility of the beam delivery system of the next linear colliders (ILC and CLIC) as well as to define and to test the tuning methods. As the design vertical beam sizes of the linear colliders are about few nanometers, the stability of the trajectory as well as the control of the aberrations are very critical. ATF2 commissioning started in December 2008, and thanks to submicron resolution beam position monitors (BPMs), it has been possible to measure the beam position fluctuation along the final focus of ATF2 during the 2009 runs. The optics was not the nominal one yet, with a lower focusing to make the tuning easier. In this paper, a method to measure the noise of each BPM every pulse, in a model-independent way, will be presented. A method to reconstruct the trajectory's fluctuations is developed which uses the previously determined BPM resolution. As this reconstruction provides a measurement of the beam energy fluctuations, it was also possible to measure the horizontal and vertical dispersion function at each BPMs parasitically. The spatial and angular dispersions can be fitted from these measurements with uncertainties comparable with usual measurements.

DOI: 10.1103/PhysRevSTAB.16.062803 PACS numbers: 29.20.Ej

I. INTRODUCTION

The future linear collider projects (ILC [1] and CLIC [2]), to have a high luminosity, must collide beams with few nanometers vertical size. It requires to create small emittance beams and to focus them to nanometers.

The Accelerator Test Facility (ATF) successfully creates beam with almost the emittances required by the ILC [3]. The ATF2 facility [4] uses the beam extracted from the ATF damping ring. It was built to demonstrate the feasibility of the beam delivery system of a future linear collider, to implement and test the instrumentation and tuning procedures involved to obtain the nanometer scale transverse beam size necessary for a high luminosity. ATF2 is a follow-up of the final focus (FF) test beam experiment at SLAC [5]. ATF2's final focus optics are scaled down from the ILC design and this is the first implementation of the local chromaticity correction scheme [6] (also used for the CLIC design). A comparison of the ATF2, ILC, and CLIC parameters is given in Table I.

The two main goals of ATF2 are to first demonstrate the ability to tune the beam down to 40 nm vertical beam size at the IP and later to control the pulse to pulse beam jitter to be lower than 4 nm at the IP. Both of these goals require the use of feedback to reduce the incoming beam jitter. Moreover, the tuning of the needed feedback algorithms depends on the characteristics of the jitter. This paper proposes a convenient method to determine it for each pulse, which has been applied during the 2009 runs.

In the final focus section (see Fig. 1), the large β functions magnify incoming beam jitter up to several microns displacement in the FF and the horizontal dispersion is large enough to convert the beam energy jitter (typically $\frac{\Delta E}{E} \sim 5 \times 10^{-5}$) up to several microns displacements too. We show that, thanks to precise cavity beam position monitors (BPMs) (with submicron resolution), it is possible to reconstruct all the incident parameters of the beam pulse by pulse. This allows not only reconstructing beam fluctuations for the purpose of stability analysis and feedback, but also measuring the dispersion functions in a noninvasive way. The latter is of particular importance as

TABLE I. Comparison of the parameters of ILC, CLIC, and ATF2.

Parameters	Symbol	ILC (500 GeV)	CLIC (3 TeV)	ATF2 (1.3 GeV)
Bunch population	N_b	2×10^{10}	4×10^{9}	$1–2 \times 10^{10}$
Number of bunches/train	n_b	2625	312	1(goal 1)–30(goal 2)
Linac repetition rate	f_{rep}	5 Hz	50 Hz	1.5 Hz
Horizontal beam size at IP	σ_x^*	640 nm	45 nm	3 μm
Vertical beam size at IP	σ_y^*	5.7 nm	1 nm	37 nm
Bunch length	σ_z	300 μm	44 μm	8 mm
Horizontal emittance	$\gamma\epsilon_x$	1000 nm rad	660 nm rad	5000 nm rad
Vertical emittance	$\gamma\epsilon_y$	40 nm rad	20 nm rad	30 nm rad
Energy loss to beamstrahlung	δ_{BS}	2.4%	29%	Nonrelevant
Peak luminosity	$\mathcal{L}_{\mathrm{pk}}$	2×10^{34} cm^2 s^{-1}	6×10^{34} cm^2 s^{-1}	Nonrelevant

part of the optical tuning of the final focus section needed to minimize the beam size at the interaction point.

After a brief description of the cavity BPMs used in ATF2 final focus, a model-independent method is used to measure the noise contribution in each BPM using a few hundred position measurements. The spatial parameters and energy fluctuation of the incoming beam are then fitted, weighted by the determined BPM resolutions. In the last section, the energy fluctuation reconstruction is used to measure the dispersion function at each BPM and then globally fitted.

II. CAVITY BPM AT ATF2

A. Instrument

There are two types of cavity BPMs in ATF2: the C-band [7] (with a resonant frequency of 6.4 GHz) and the larger aperture S-band [8] (2.9 GHz). Both types share the same operation principle [9] and they are attached to quadrupoles and sextupoles in the extraction line and in the final focus. In the final focus each quadrupole and sextupole is placed on a mover allowing horizontal and vertical displacements as well as roll with respectively a few micrometers and a few microradians resolution (see Fig. 2).

Each cavity BPM is composed by a cylindrical cavity and four waveguides. The cavity and the waveguides are connected by slots placed on the end plate of the cavity.

When the beam goes through the cavity with an offset, the TM_{110} mode, also called dipole mode, is excited proportionally to the product of offset and charge [10]. That dipole mode signal in the sensor cavity is selectively fed out to the waveguides through slots via magnetic coupling.

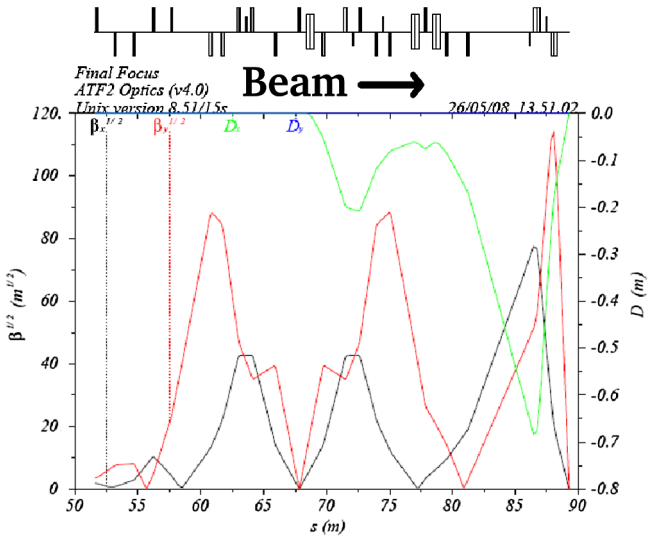

FIG. 1. Nominal ATF2 final focus optics.

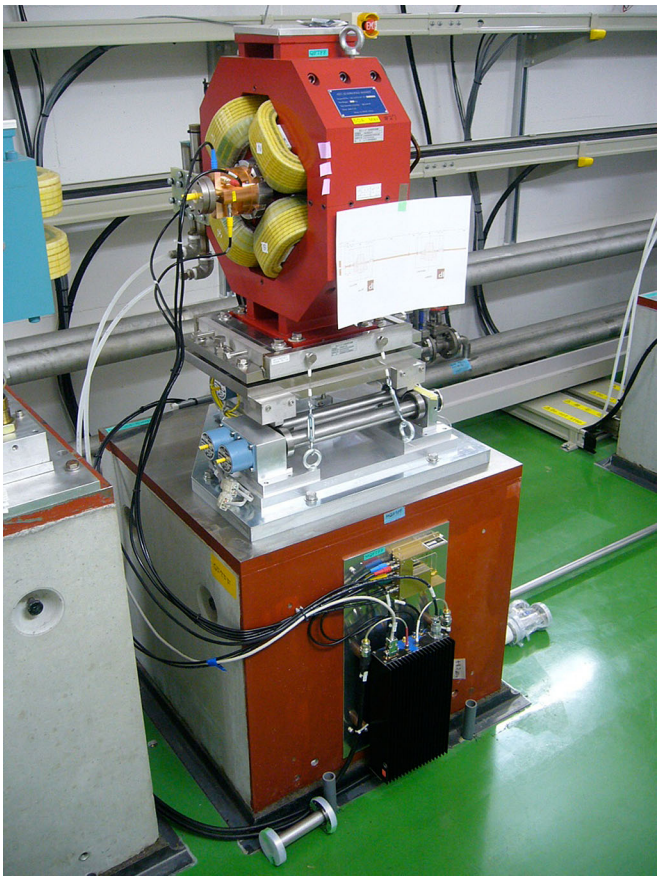

FIG. 2. A C-band BPM inside of a quadrupole on a mover.

Then antennas on the waveguides pick the signal up into coaxial cables.

B. Electronics and readout

The signals are summed in a 180° hybrid, to increase the signal level and remove any common mode left after the selective waveguide couplers. The signals are then mixed down to ≃20 MHz in custom radio frequency electronics in a single stage heterodyne system. The amplitude and phase of the resulting signal is measured paying attention to the saturation.

To infer the beam position from the signal amplitude, the cavity has to be calibrated. The calibration is achieved by moving the cavity by a known amount using the mover and measuring the amplitude variation. For the cavities in the extraction line, as the corresponding quadrupole is not on a mover, a beam bump technique is used for the calibration.

To avoid saturation, 20 dB attenuators have been installed, increasing so the dynamic range of the cavity from 500 μm to 5 mm but also degrading the resolution (300 nm instead of 30 nm).

The digitized signals are further digitally down-mixed to obtain amplitude and phase information. Calibration constants are applied on-line and the full orbit supplied to the ATF2 control system and flight simulator [11].

III. BPMS NOISE LEVEL MEASUREMENT

A. Model-independent measurement method

Each BPM measurement is affected by noise, mainly from the electronics. To measure BPM resolutions, a large set of measured trajectories can be used, looking for correlations between the different BPMs [12]. Unlike traditional model-independent analysis (MIA) as in [13], the presented method does not require to analyze singular vectors which is why it can be more easily automated, but it also means it is less precise, as nonphysical dynamics can be accounted for. Since the noise measurements is here mainly used as a weighting for other fits, this simplified method was enough.

The noise at one BPM is, by definition, uncorrelated with that of other BPMs, unlike the beam positions, which are usually correlated because they are related by the transfer matrices. Hence, one can write with m BPMs:

$$X_{\mathrm{BPM1}}(i) = \sum_{j=2}^{m}[\delta x_j \cdot X_{\mathrm{BPM}j}(i) + \alpha x_j] + \sum_{j=2}^{m}[\delta y_j \cdot Y_{\mathrm{BPM}j}(i) + \alpha y_j] + N_i, \quad (1)$$

where $X_{\mathrm{BPM}j}(i)$ [respectively $X_{\mathrm{BPM}j}(i)$] corresponds to the horizontal (respectively vertical) measurement at the jth BPM for the ith pulse; δx_j (respectively δx_j) and αx_j (respectively αy_j) are the linear relation coefficients between the horizontal measurement of the first BPM and the horizontal (respectively vertical) measurement of the jth BPM; N_i is the noise value of the first BPM for the ith pulse in the horizontal plane.

From Eq. (1), with n pulses, we obtain Eq. (2):

$$\begin{pmatrix} X_{\mathrm{BPM}\,1}(1) \\ \vdots \\ X_{\mathrm{BPM}\,1}(n) \end{pmatrix} = \begin{pmatrix} X_{\mathrm{BPM}\,2}(1) & \cdots & X_{\mathrm{BPM}\,m}(1) & Y_{\mathrm{BPM}\,2}(1) & \cdots & Y_{\mathrm{BPM}\,m}(1) & 1 \\ & \vdots & & & \vdots & & \\ X_{\mathrm{BPM}\,2}(n) & \cdots & X_{\mathrm{BPM}\,m}(n) & Y_{\mathrm{BPM}\,2}(n) & \cdots & Y_{\mathrm{BPM}\,m}(n) & 1 \end{pmatrix} \times \begin{pmatrix} \delta x_2 \\ \vdots \\ \delta x_m \\ \delta y_2 \\ \vdots \\ \delta y_m \\ \alpha \end{pmatrix} + \begin{pmatrix} N_1 \\ \vdots \\ N_n \end{pmatrix},$$

$$\text{where } \alpha = \sum_{j=2}^{m} \alpha x_j + \alpha y_j. \quad (2)$$

Let us call B_1 the vector of the first BPM readings, B_{all} this big matrix of all BPM readings except the first, Δ the vector containing the $m-1$ coefficients δx and δy as well as the coefficient α, and $N(\mathrm{BPM}_1)$ the vector containing the noise amplitude at each pulse for the first BPM. So, Eq. (2) becomes

$$B_1 = B_{\mathrm{all}} \cdot \Delta + N(\mathrm{BPM}_1). \quad (3)$$

Since the noise is random, we can have an estimation of Δ:

$$\Delta = B_{\mathrm{all}}^{-1} \cdot B_1. \quad (4)$$

The vector $N(\mathrm{BPM}_1)$ containing the noise amplitude at each pulse for the first BPM can be obtained by this relation:

$$N(\mathrm{BPM}_1) = B_1 - B_{\mathrm{all}} \cdot (B_{\mathrm{all}}^{-1} \cdot B_1). \quad (5)$$

The norm of the $N(\mathrm{BPM}_1)$ vector, equal to the rms of the noise amplitudes $X_{\mathrm{err}}(\mathrm{BPM}_1)$, will give the resolution of the first BPM (under the assumption the resolution is limited by the noise). The same method is then applied for each BPM in the horizontal and vertical planes. However, the noise level must be similar for all the BPMs, or we get precision issues when inverting the B_{all} matrix. That means, in case of a beam line including different BPM designs, this method must be applied for each design separately.

B. Experimental BPM noise level measurement at ATF2

The resolution measurements are presented in blue in Fig. 4. 300 pulses keeping the same optics were used for this analysis.

The measured resolution of the C-Band cavity BPMs is between 500 nm and 1 μm in the horizontal plane and 400 nm in the vertical one.

As beam based alignment had not yet implemented for sextupoles, the alignment of the corresponding cavities was poorer than in the quadrupoles. This may have led the beam offset to be near the limit of the dynamic range of the cavity, thus explaining the difference in resolution seen in Fig. 4. The larger resolution observed for some BPMs not attached to quadrupoles on mover may be due to the calibration method, which uses beam bumps and is much less precise than for quadrupoles on mover.

This method is model independent which means it does not rely on the transfer matrices. It also automatically takes into account the roll of the BPMs.

IV. TRAJECTORY FLUCTUATION RECONSTRUCTION

A. Fluctuations reconstruction principle

It is possible to predict the beam position all along a beam line from six parameters of the beam at the injection point (x, x', y, y', z, $\frac{dE}{E}$) and the knowledge of the transfer matrices from that injection point. As there is neither cavities nor chicanes in ATF2, the z parameter has no effect and will not be used in this paper.

As the sextupoles were turned off during the 2009 runs, the transverse beam dynamics is supposed linear. The transfer matrices are computed by optics codes from the magnetic lattice.

From position measurement along the beam line, one can reconstruct the parameters of the beam for example at the injection [inverting Eq. (6)] and even propagate them back to obtain a trajectory reconstruction which is easily comparable to the BPMs measurement [applying Eq. (6) to the parameters found]:

$$\begin{pmatrix} \Delta x(\mathrm{BPM}_1) \\ \vdots \\ \Delta x(\mathrm{BPM}_n) \\ \Delta y(\mathrm{BPM}_1) \\ \vdots \\ \Delta y(\mathrm{BPM}_n) \end{pmatrix} = \begin{pmatrix} R_{11}(\mathrm{injection} \rightarrow \mathrm{BPM}_1) & \cdots & R_{16}(\mathrm{injection} \rightarrow \mathrm{BPM}_1) \\ \vdots & & \vdots \\ R_{11}(\mathrm{injection} \rightarrow \mathrm{BPM}_n) & \cdots & R_{16}(\mathrm{injection} \rightarrow \mathrm{BPM}_n) \\ R_{31}(\mathrm{injection} \rightarrow \mathrm{BPM}_1) & \cdots & R_{36}(\mathrm{injection} \rightarrow \mathrm{BPM}_1) \\ \vdots & & \vdots \\ R_{31}(\mathrm{injection} \rightarrow \mathrm{BPM}_n) & \cdots & R_{36}(\mathrm{injection} \rightarrow \mathrm{BPM}_n) \end{pmatrix} \times \begin{pmatrix} \Delta x \\ \Delta xp \\ \Delta y \\ \Delta yp \\ \frac{\Delta E}{E} \end{pmatrix}_{\mathrm{injection}} . \quad (6)$$

We will use the notation $\Delta XY = M \times P$ for Eq. (6).

The reconstruction is done by a least square minimization with

$$\chi^2 = \|(\Delta XY - M \times P)^T \times (\Delta XY - M \times P)\|. \quad (7)$$

The BPM resolutions X_{err} and Y_{err} obtained as described above can be used as weight. Using the notation W for the diagonal matrix with elements

$$w_{ii} = \begin{cases} \frac{1}{X_{\mathrm{err}}(\mathrm{BPM}_i)^2} & \text{if } i \leq n \\ \frac{1}{Y_{\mathrm{err}}(\mathrm{BPM}_{i-n})^2} & \text{if } i > n, \end{cases} \quad (8)$$

the χ^2 becomes

$$\chi^2 = \|(\Delta XY - M \times P)^T \times W \times (\Delta XY - M \times P)\|. \quad (9)$$

B. Parameters reconstruction changing beam energy

To test this reconstruction, trajectory data were taken during a dispersion measurement changing the ring cavity frequency (RCF) to vary the beam energy. The parameters were reconstructed using the injection point as reference. The time evolution of these reconstructed parameters is shown in Fig. 3. The fit was done using the cavity BPMs with the resolutions determined as described in the previous section. The trajectory, deduced from the fitted parameters, was then computed for all BPMs.

The different RCF steps, applied during the dispersion measurement, are clearly visible on the energy curve and correspond to the values expected from the frequency change (in dashed light blue). One can also see a correlation of the energy with X, which indicates the presence of horizontal dispersion at the injection point.

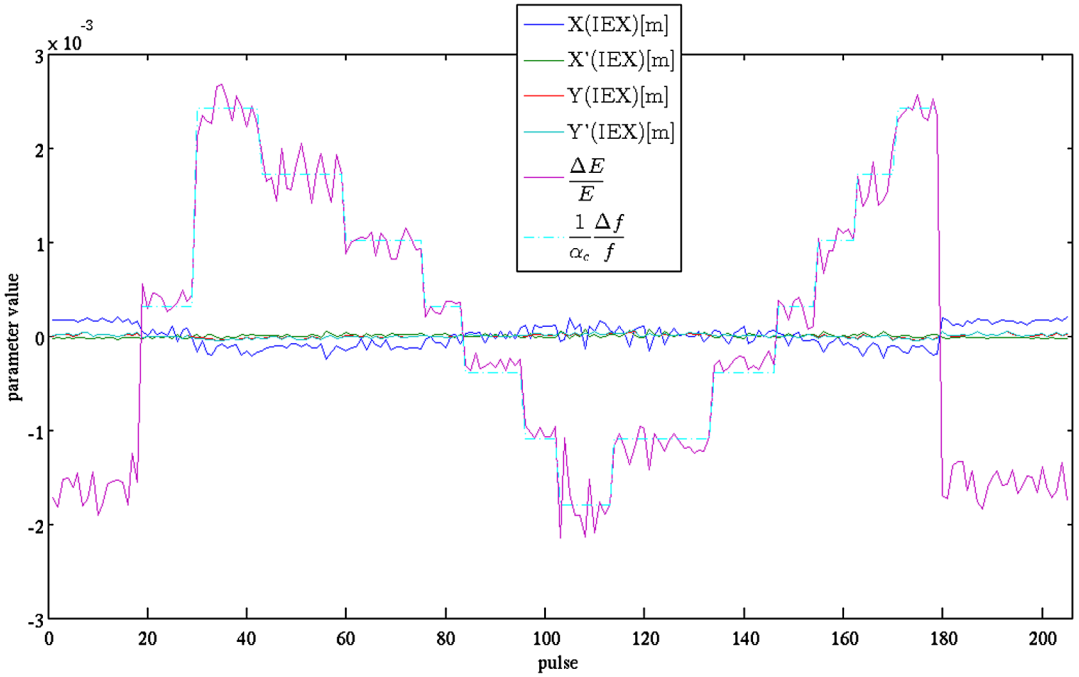

FIG. 3. Reconstruction of the parameters at the injection point during a dispersion measurement.

C. Fluctuations reconstruction

The reconstruction of the fluctuations of the trajectory in periods when no change was applied was shown to also be possible. The same data as for the BPM resolution measurements presented in the previous section has been used for that.

We saw that we can compute the BPM noise at each pulse N, if we subtract it from the BPM measurement ΔX_{read}, we get the real position ΔX of the beam with respect to the electrical center of the BPM: $\Delta X = \Delta X_{\text{read}} - N$.

To appreciate the precision achievable with this reconstruction, we compute for each BPM $\sqrt{\sum_{\text{pulses}}(\Delta X - \Delta X_{\text{reco}})^2}$ the quadratic sum of the beam position minus the reconstructed trajectory, and plot it as the fit precision along with the resolution of the BPM for horizontal and vertical displacements (Fig. 4). The cavity BPMs attached to a quadrupole on mover (from MQ16FF to MQD2AFF) were used for this reconstruction.

We can see that the fit precision is a few microns in horizontal cavity BPMs and essentially below 1 μm in the vertical plane. The statistical error can be estimated to be about the resolutions of the BPMs divided by the square root of the number of BPMs used corresponding to $\simeq \frac{0.5}{\sqrt{20}} \simeq 0.1$ μm. As this statistical error is much below the fit precision, it means that the precision is limited by systematics such as errors on the transfer matrices, BPM scale factors, or BPMs rotations. The fit resolution becomes bad for the MQF19X to MQF21X BPMs in the horizontal plane: as they are not on movers, their calibrations are more difficult possibly resulting in larger scale errors.

The characterization of this jitter at the injection has been done and the histogram of the energy jitter is presented in Fig. 5. The energy jitter was really low (2×10^{-5}). In the past, amplitudes of about 8×10^{-5} have been measured [14].

V. DISPERSION RECONSTRUCTION

A. Method

The dispersion functions $D_x(s)$ and $D_y(s)$ describe the beam position displacement correlated to the energy whereas angular dispersion functions $D'_x(s)$ and $D'_y(s)$ describe the angular displacement correlated to the energy:

$$\frac{\partial \Delta X(s)}{\partial \frac{\Delta E}{E}} = D_x(s), \qquad \frac{\partial \Delta Y(s)}{\partial \frac{\Delta E}{E}} = D_y(s),$$
$$\frac{\partial \Delta X(s)'}{\partial \frac{\Delta E}{E}} = D'_x(s), \qquad \frac{\partial \Delta Y(s)'}{\partial \frac{\Delta E}{E}} = D'_y(s).$$

We saw that we are able to reconstruct the pulse to pulse energy fluctuations. The correlation between the energy reconstruction and the BPM position measurements allows measuring the dispersion at each BPM. We have, with $R_{ij} = R_{ij}(\text{ref} \rightarrow \text{BPM})$,

$$\Delta X(\text{BPM}) = R_{11} \times X(\text{ref}) + R_{12} \times X'(\text{ref}) + R_{13} \times Y(\text{ref}) + R_{14} \times Y'(\text{ref}) + R_{16} \times \frac{\Delta E}{E}. \tag{10}$$

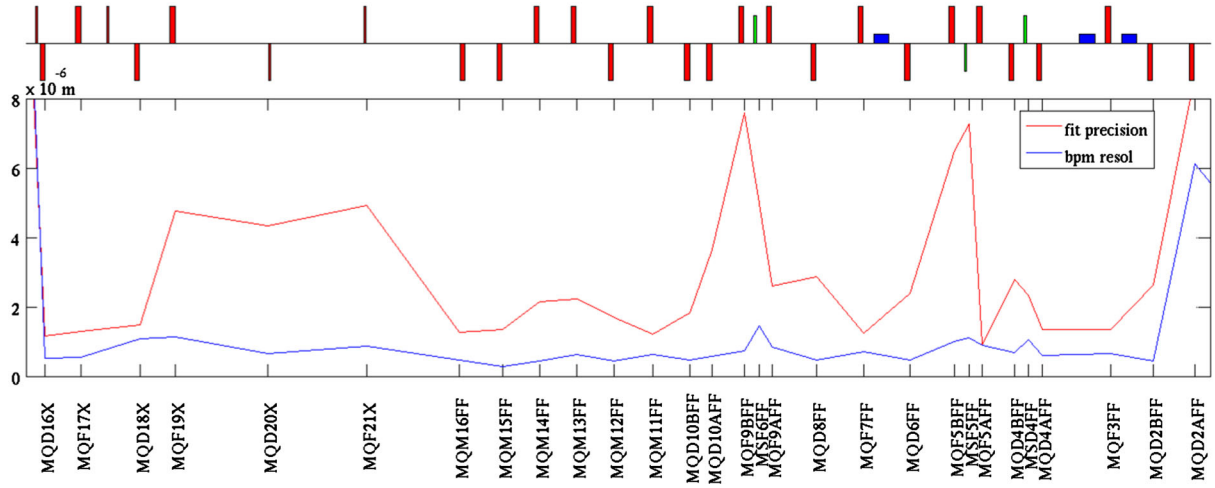

(a) Horizontal C-band cavity BPMs

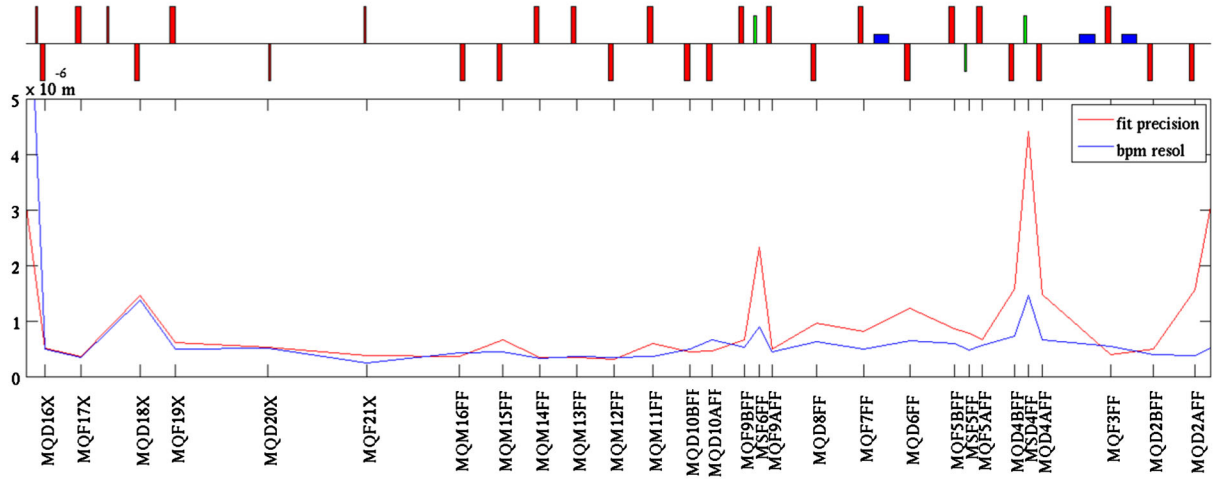

(b) Vertical C-band cavity BPMs

FIG. 4. Horizontal and vertical resolution of the BPMs along with the fit resolution.

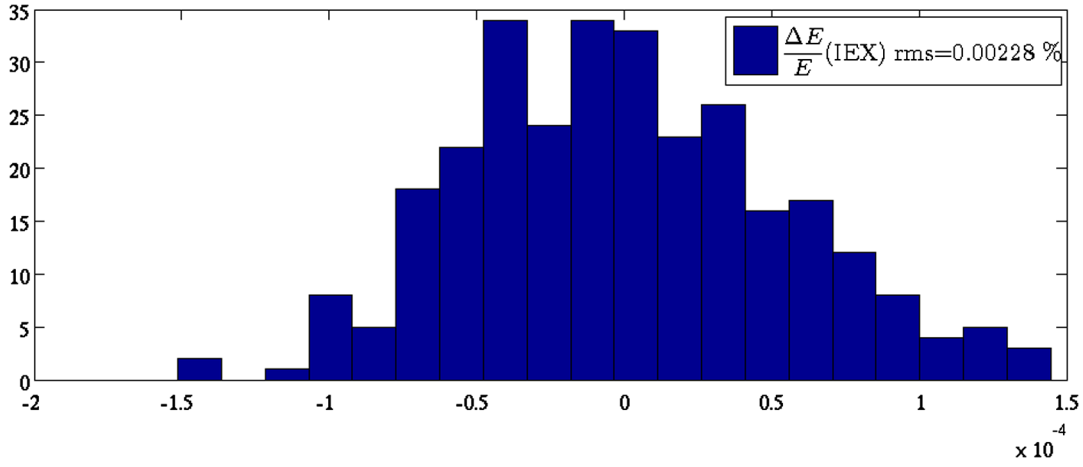

FIG. 5. Energy jitter reconstructed.

The correlation between the position and the energy can be separated as shown [Eq. (11)]:

$$\begin{aligned} D_x(\mathrm{BPM}) &= \frac{\partial \Delta X(\mathrm{BPM})}{\partial \frac{\Delta E}{E}} \\ &= R_{16} + \frac{\partial X(\mathrm{ref})}{\partial \frac{\Delta E}{E}} \times R_{11} + \frac{\partial X'(\mathrm{ref})}{\partial \frac{\Delta E}{E}} \times R_{12} + \frac{\partial Y(\mathrm{ref})}{\partial \frac{\Delta E}{E}} \times R_{13} + \frac{\partial Y'(\mathrm{ref})}{\partial \frac{\Delta E}{E}} \times R_{14} D_{x\,\mathrm{mod}}(\mathrm{BPM}) \\ &\quad + D_x(\mathrm{ref}) \times R_{11} + D'_x(\mathrm{ref}) \times R_{12} + D_y(\mathrm{ref}) \times R_{13} + D'_y(\mathrm{ref}) \times R_{14}. \end{aligned} \tag{11}$$

That means that the measured dispersion is a combination of the model dispersion and the propagation of the mismatched dispersion from injection.

To calculate the spatial and angular dispersion at a reference point $D(\mathrm{ref})$ from the difference ΔD between the measured spatial dispersion at each of the n BPM (D_x and D_y) and the modeled ones ($D_{x\,\mathrm{mod}}$ and $D_{y\,\mathrm{mod}}$), we must solve

$$\Delta D = M \times D(\mathrm{ref}) \tag{12}$$

with

$$\Delta D = \begin{pmatrix} D_x(\mathrm{BPM}_1) - D_{x\,\mathrm{mod}}(\mathrm{BPM}_1) \\ \vdots \\ D_x(\mathrm{BPM}_n) - D_{x\,\mathrm{mod}}(\mathrm{BPM}_n) \\ D_y(\mathrm{BPM}_1) - D_{y\,\mathrm{mod}}(\mathrm{BPM}_1) \\ \vdots \\ D_y(\mathrm{BPM}_n) - D_{y\,\mathrm{mod}}(\mathrm{BPM}_n) \end{pmatrix}, \quad M = \begin{pmatrix} R_{11}(\mathrm{BPM}_1) & \cdots & R_{14}(\mathrm{BPM}_1) \\ \vdots & & \vdots \\ R_{11}(\mathrm{BPM}_n) & \cdots & R_{14}(\mathrm{BPM}_n) \\ R_{31}(\mathrm{BPM}_1) & \cdots & R_{34}(\mathrm{BPM}_1) \\ \vdots & & \vdots \\ R_{31}(\mathrm{BPM}_n) & \cdots & R_{34}(\mathrm{BPM}_n) \end{pmatrix}, \quad R_{ij}(\mathrm{BPM}_k) = R_{ij}(\mathrm{ref} \rightarrow \mathrm{BPM}_k),$$

and

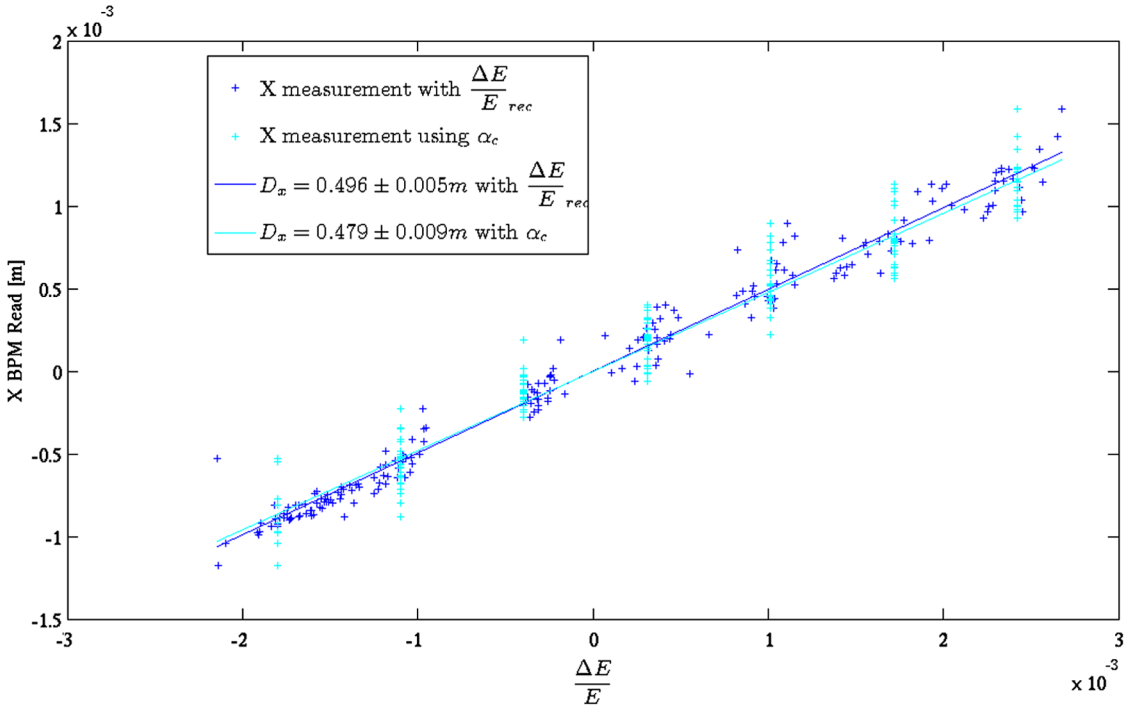

FIG. 6. Two methods for horizontal dispersion fit at MQF1X.

$$D(\text{ref}) = \begin{pmatrix} D_x(\text{ref}) \\ D'_x(\text{ref}) \\ D_y(\text{ref}) \\ D'_y(\text{ref}) \end{pmatrix}.$$

To solve this equation, we use least square minimization. The horizontal and vertical dispersions are measured at each BPM through a linear fit of the beam positions function of the energy. The errors D_{err}, on the measured dispersion D obtained by these fits, are used in the least square minimization [as shown in Eq. (9)].

The energy change can be determined by (i) changing the RCF and using the momentum compaction factor [Eq. (13)],

$$\frac{\Delta p}{p} = \frac{\gamma^2}{1 - \alpha_c \gamma^2} \frac{\Delta f_{\text{ring}}}{f_{\text{ring}}} \simeq -\frac{1}{\alpha_c} \frac{\Delta f_{\text{ring}}}{f_{\text{ring}}}, \qquad (13)$$

and (ii) using the energy jitter from the beam parameter reconstruction (see previous section) in a similar way as it has been done in the Stanford Linear Collider [15].

B. Comparison of two dispersion reconstruction methods

Using the data displayed in Fig. 3, where the energy had been changed using the RCF, we fit the dispersion at all BPMs. In Fig. 6, the two methods to determine the energy variation are applied, and the horizontal displacement function of the energy variation is plotted for both. The horizontal dispersion is then fitted separately for the two methods. One can see the energy value from the reconstruction and the one obtained using the momentum compaction factor agree well. As the dispersion obtained from the reconstruction is a bit more precise and as it makes the analysis easier, the energy will be obtained that way from now on.

From the measurements of the dispersions in the BPMs, the fit of the incoming spatial and angular dispersion at the injection point is deduced by least square minimization [Eq. (12)]. The incoming dispersion is then propagated along the beam line to be compared with the individual BPM measurements as shown in Fig. 7.

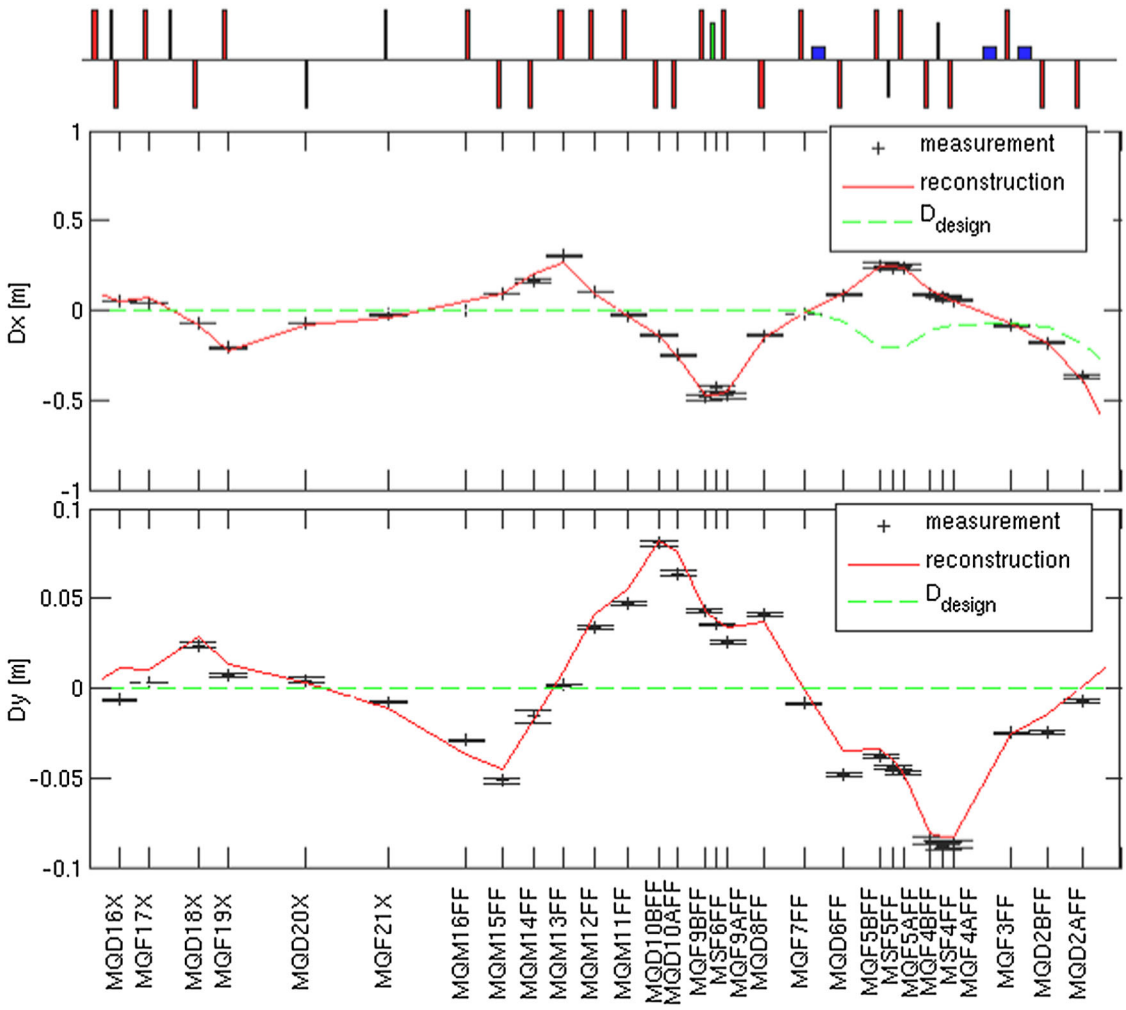

FIG. 7. Reconstructed dispersion compared to individual BPM measurements based on changing the RCF.

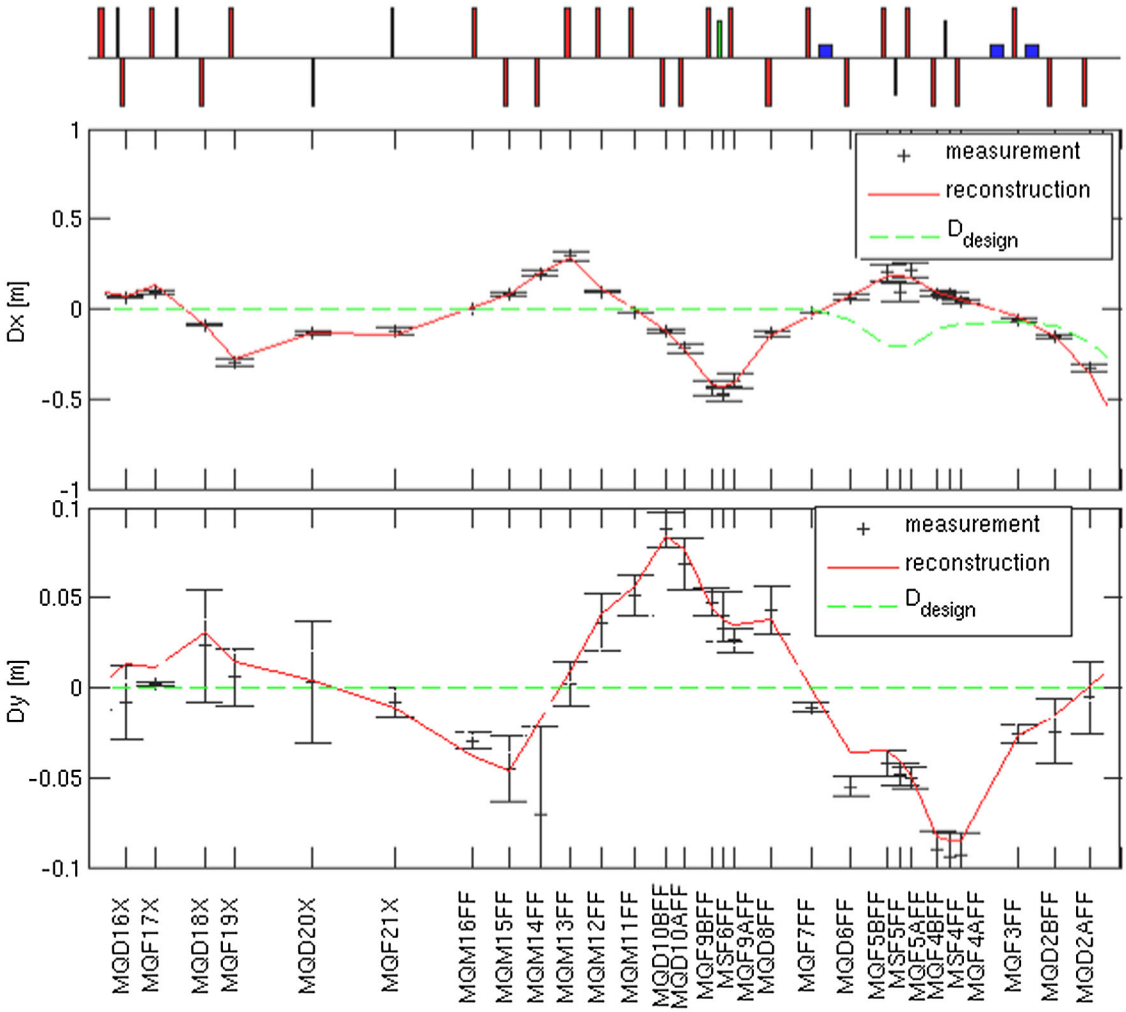

FIG. 8. Reconstructed dispersion compared to individual BPM measurements based on using beam fluctuations.

This method has the advantage to reduce the systematic errors compared with methods based on single position measurements.

The same measurement has been made with beam jitter (without changing the RCF). The results are shown in Fig. 8.

We can see that the fit is consistent with most of the individual horizontal and vertical measurements. The dispersion measurements are very close with the two methods (see Table II). The data, which was taken before implementing any dispersion correction, shows a significant leakage propagating along the entire line. This explains the large differences with the design values.

TABLE II. Comparison of the two dispersion fit methods using the IP as reference point.

Measurement	Changing RCF	From fluctuation
D_x(IP) [mm]	-127 ± 1	-131 ± 1
D'_x(IP) [mrad]	271 ± 1	278 ± 1
D_y(IP) [mm]	29 ± 3	24 ± 3
D'_y(IP) [mrad]	-67 ± 8	-58 ± 6

One can see that the errors on the measurements do not depend on the choice of the method. The reason for that is that the reconstructed dispersion at injection is dominated by the systematic errors (BPMs scales factors, transfer matrices estimation, etc.).

The criteria for a good dispersion correction can be deduced from the influence of the dispersion on the beam size (notation σ_{tot} for the beam size with the dispersion effect and σ_{mono} for the monochromatic beam size).

For example to calculate the dispersion $D_{\max}$ at IP, which increases the beam size by $r = 10\%$ at IP, as we have

$$\sigma_{\text{tot}} = \sqrt{\sigma_{\text{mono}}^2 + \left(D\frac{\Delta E}{E}\right)^2},$$

we get

$$r = \frac{\sigma_{\text{tot}}}{\sigma_{\text{mono}}} - 1 = \sqrt{1 + \left(\frac{D_{\max}\frac{\Delta E}{E}}{\sigma_{\text{mono}}}\right)^2} - 1 \simeq \left(\frac{D_{\max}\frac{\Delta E}{E}}{2\sigma_{\text{mono}}}\right)^2$$

$$\text{if } D_{\max}\frac{\Delta E}{E} \ll \sigma_{\text{mono}}.$$

So,

$$D_{\max} = 2\frac{\sqrt{r}\sigma_{\text{mono}}}{\frac{\Delta E}{E}}. \quad (14)$$

From Eq. (14) we deduce, for $r = 10\%$ and nominal optics, that the dispersion must not exceed $D_{x\max} = 10$ mm and $D_{y\max} = 1$ mm. As the measurements of the dispersion show a few mm precision (Table II), this measurement alone is not precise enough to correct fully the dispersion. However after correction, the dispersion would be well within the range achievable using sextupole displacement knob and looking at the beam size.

VI. CONCLUSION AND PROSPECTS

After a quick presentation of the cavity BPMs used at ATF2, a model-independent method to obtain the noise level of BPMs directly from measurements has been presented. It has been used to determine the resolution of ATF2's cavity BPMs (below 1 μm in both planes during the initial period when they were used with 20 dB attenuators, corresponding to the expectations). This resolution allowed the reconstruction of pulse to pulse trajectory variations with a precision estimated to be a few microns in the horizontal plane and below 1 μm in the vertical plane. These results are limited by the knowledge of the transfer matrices and the BPM calibrations.

As the fluctuation reconstruction gives the energy deviation for each pulse, it was shown how to measure the dispersion at each BPM in a noninvasive way, using the natural fluctuations of the beam energy, and how to fit the dispersion along the beam line from these results. These measurements have been shown to be as precise as the more classic measurement obtained changing the beam energy manually, with a precision of a few millimeters for the spatial dispersion and of a few milliradians for the angular dispersion (values are optics dependent), with the same limitations as for the reconstruction of the fluctuations.

From these results, it appears that an effort has to be done to improve the knowledge of the transfer matrices and to calibrate the BPMs attached to quadrupoles which are not on movers, in order to be able to use the cavity BPMs at their full potential, especially since the attenuators have been removed from most of the cavity BPMs, thus giving access to 30 nm resolution.

A further development of the techniques described in this paper is also expected to enable resolving ground motion effects during the beam trajectory measurements as well as higher order contributions to the beam transfer. Both effects are estimated to contribute at the level of a few microns to the measured trajectories and are currently part of the systematics in our method. Resolving the nonlinearities along the final focus lattice will be useful to check their overall cancellation in the chromatic correction section.

ACKNOWLEDGMENTS

We thank the ATF/ATF2 collaboration for its help and support. We acknowledge as well the support of the Agence Nationale de la Recherche of the French Ministry of Research (Programme Blanc, Project No. ATF2-IN2P3-KEK, Contract No. ANR-06-BLAN-0027).

[1] James Brau *et al.*, International Linear Collider Report No. ILC-REPORT-2007-001.
[2] R Tomàs, Phys. Rev. ST Accel. Beams **13**, 014801 (2010).
[3] Y. Honda *et al.*, Phys. Rev. Lett. **92**, 054802 (2004).
[4] Boris Ivanovich Grishanov *et al.*, ATF2 Report No SLAC-R-771.
[5] M. Berndt *et al.*, Report No. SLAC-0376 [http://www.slac.stanford.edu/cgi-wrap/getdoc/slac-r-376.pdf].
[6] P. Raimondi and A. Seryi, Phys. Rev. Lett. **86**, 3779 (2001).
[7] A. Lyapin, B. Maiheu, M. Wing, S. Shin, Y. Honda, T. Tauchi, N. Terunuma, A. Heo, E. Kim, K. Kim, R. C. E. Ainsworth, S. T. Boogert, G. Boorman, S. Molloy, D. McCormick, J. Nelson, G. White, and D. Ward, Report. No. EuCARD-CON-2009-005, 2009 [http://cdsweb.cern.ch/record/1225901/files/EuCARD-CON-2009-005.pdf].
[8] A. Lyapin, B. Maiheu, M. Wing, S. Shin, Y. Honda, T. Tauchi, N. Terunuma, A. Heo, E. Kim, K. Kim, R. C. E. Ainsworth, S. T. Boogert, G. Boorman, S. Molloy, D. McCormick, J. Nelson, G. White, and D. Ward, in *Proceedings of the 23rd Particle Accelerator Conference, Vancouver, Canada, 2009* (IEEE, Piscataway, NJ, 2009) [http://trshare.triumf.ca/~pac09proc/Proceedings/papers/th6rep025.pdf].
[9] S. T. Boogert, R. Ainsworth, G. Boorman, S. Molloy, M. Ross, A. Aryshev, Y. Honda, N. Terunuma, J. Urakawa, E. S. Kim, Y. I. Kim, A. E. Heo, A. Lyapin, C. J. Swinson, J. Frisch, D. M. McCormick, J. Nelson, T. Smith, and G. R White, Report. No. EuCARD-CON-2010-028, 2010 [http://cds.cern.ch/record/1299158/files/EuCARD-CON-2010-028.pdf].
[10] Sean Walston *et al.*, Nucl. Instrum. Methods Phys. Res., Sect. A **578**, 1 (2007).
[11] G. White, S. Molloy, A. Seryi, D. Schulte, R. Tomas, S. Kuroda, P. Bambade, and Y. Renier, in *Proceedings of the 11th European Particle Accelerator Conference, Genoa, 2008* (EPS-AG, Genoa, Italy, 2008), pp. 1562–1564 [http://accelconf.web.cern.ch/accelconf/e08/papers/tupp016.pdf].
[12] M. Slater *et al.*, Nucl. Instrum. Methods Phys. Res., Sect. A **592**, 201 (2008).
[13] Chun-xi Wang, John Irwin, Karl Bane, Yunhai Cai, Franz J. Decker *et al.*, Report. No. SLAC-PUB-7909, 2003.
[14] K. Kubo, Report No. ATF-99-11, 1999 [http://atf.kek.jp/collab/ap/library/internal-reports/ATF-99-11.pdf].
[15] P. Emma, T. H. Fieguth, and T. Lohse, Nucl. Instrum. Methods Phys. Res., Sect. A **288**, 313 (1990).